Defect Inspection of Quartz-PSMs: Taking a Leap Forward

J. Heumann[*a], F. Schurack[a], W. Dettmann[b], L. Zurbrick [**c], M. Lang[c]
[a] - Advanced Mask Technology Center, Rähnitzer Allee 9, 01109 Dresden, Germany
[b] - Infineon Technologies AG, Balanstrasse 73, 81541 Munich, Germany
[c] - KLA-Tencor Corporation, 160 Rio Robles, San Jose, CA 95134-1809, USA

ABSTRACT

Defect inspection of Quartz-PSMs is challenging, as the optical contrast for defects within the quartz substrate is small. The performance of three phase contrast algorithms is studied with a variety of defect test masks. For alternating phase shift masks key parameters such as optimum focus offset, defect sensitivity for different feature sizes, as well as defect sensitivity with respect to defect printability criteria are studied. It was found that the defect sensitivity of one of the algorithms exhibits a dependence on feature size. For the other two algorithms in the studied range the defect sensitivity is independent of the feature size. In focus runs performed on large feature sizes a single optimum focus offset is observed, whereas for small feature sizes a two-path inspection using a positive and negative focus offset is found necessary. With respect to defect printability all critical 180° defects were found. For the newest of the three algorithms good inspectability of chrome-less PSMs is achieved.

Keywords: Phase shift masks, quartz defects, mask inspection, defect printability

1 INTRODUCTION

Alternating as well as chrome-less phase shift masks (PSMs) are promising resolution enhancement techniques (RETs) to realize smaller design rules at the same lithography wavelength[1,2]. Both mask types fall into the category of quartz phase shift masks (Quartz-PSMs) as they use the quartz substrate to generate a local phase shift of the incoming light.

The production of Quartz-PSMs requires etching of the quartz substrate, which can cause possible quartz defects. For the successful implementation of Quartz-PSMs into the wafer manufacturing process the production of defect free reticles is critical[3,4]. To assure a high reticle quality the defect inspection needs sufficient quartz defect sensitivity. Defect inspection of Quartz-PSMs is challenging, as the optical contrast for defects within the quartz substrate is smaller than for defects in the chrome layer.

The inspection of Quartz-PSMs has been an evolutionary process. At first already existing UV inspection tools, which were operating in transmitted light only, were tested for quartz defect sensitivity[5]. In order to improve the quartz defect sensitivity, a defect detection algorithm utilizing a combination of transmitted and reflected light was developed[5]. As the algorithm exhibited a feature sized depend quartz defect sensitivity, the achieved sensitivity was too low for sub 100 nm wafer design rules[6]. A leap forward in quartz defect sensitivity was taken with the development of phase contrast hardware and algorithms[7].

In this paper three phase contrast algorithms, which have been developed by KLA-Tencor especially for the detection of quartz defects, are being studied. These are “TeraPhase 400” (TPh 400) and “TeraPhase 401S” (TPh 401S), which are available for the KLA SLF platform[8,9], as well as “TeraPhase 501” (TPh 501) developed for the KLA 5xx platform. AltPSMs as well as chrome-less test masks with programmed defects were manufactured to study the performance of the TeraPhase algorithms. For all test masks a background pattern consisting of so-called “lines and spaces” with an aspect ratio of 1:1 was chosen, as in a previous study this pattern had exhibited the highest defect printability[6]. The defect sensitivity of these three algorithms is studied for different feature sizes. A defect printability study was performed, to allow for a direct comparison of the achieved and required quartz defect sensitivity.

[*] jan.heumann@amtc-dresden.com; phone +49-351-4048-264; fax +49-351-4048-9264; Advanced Mask Technology Center, Rähnitzer Allee 9, 01109 Dresden, Germany; [**] larry.zurbrick@kla-tencor.com; phone +1-408-875-6222; fax +1-408-875-4262; KLA-Tencor, 160 Rio Robles, San Jose, CA 95134-1809, USA

2 EXPERIMENTAL

All test masks contained programmed defects, which were characterized by their defect height and their lateral defect area. The defect height was measured with an atomic force microscope (AFM) and is expressed in the phase shift experienced by the incoming light relative to the defect-free quartz area. The lateral defect area was determined with the help of a scanning electron microscope (SEM) image and is measured by the square root of the estimated defect area. This so-called "square root of the area" (SRA) method was selected as in a previous study it had proven to correlate very well with the AIMS intensity deviation[6].

Furthermore measurements were being done with an "aerial imaging microscope system" (AIMS) and a printability study was being conducted. The defect's aerial image was expressed in the percentile intensity deviation measured at the defective area. The defect printability was measured by the percentile CD variation caused at the defective area. In both cases a defect-free area served as the reference value. In this paper we will only present results for on-edge quartz bumps, as they are the predominant defect type, which occurs on a production mask.

2.1 ALTERNATING PHASE SHIFT MASKS

The altPSMs consisted of chrome lines separated by a clear area (space). Every second space was etched such that there existed a 180° phase-shift between the etched and un-etched quartz areas. On-edge quartz bumps of different sizes were programmed into the etched quartz spaces (see Fig. 1). Typical defect heights of 180°, 90°, 60°, and 30° are generated through a multi-etch process. The altPSM test masks were manufactured for feature sizes of 560 nm, 440 nm, and 360 nm.

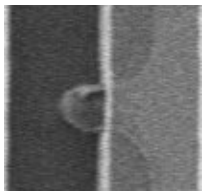

Fig. 1: On top SEM image of a 180° on-edge quartz bump.

For the defect printability test masks programmed defects of 180° were being used only. As defect printability studies are time consuming, they were performed for feature sizes of 360 nm only.

2.2 CHROME-LESS PHASE SHIFT MASKS

In an early study the inspectability of chrome-less PSMs was studied. The mask contained etched and un-etched quartz lines with a feature size of 560 nm. Destructive interference of the incident light at the transition from the etched to the un-etched quartz generates a dark line. As every edge transition generates a dark line the feature size on the wafer is cut in half. The wafer image would thus be similar to the one from an altPSM with feature sizes of 270 nm. Into the etched quartz areas different types of 180° quartz bumps were programmed.

3 DISCUSSION

3.1 FOCUS RUNS FOR TERAPHASE ALGORITHMS

The detectability of quartz defects is very much determined by the focus position of the imaging optics. Whereas chrome defects have their maximum detectability at the optimum focus, quartz defects reach their maximum detectability, when moving the optics out of the optimum focus position.

To achieve optimum quartz defect sensitivity the TeraPhase algorithms allow for the imaging optics to be moved out of its best focus with a predefined focus offset. The optimum focus offset is determined by changing the focus offset in fixed intervals, while keeping the inspection tool's sensitivity settings fixed. For each focus setting ten inspections were performed to determine the defect statistics for the specific tool settings. Finally for each defect type the capture rate of the smallest detected defect is plotted against the focus offset. The maximum of each curve represents the optimum focus offset for this particular defect type.

Focus runs were performed for the TPh 400, 401S, and 501 algorithms using altPSMs. In this section only results of TPh 400 and 501 are presented, as the performance of TPh 401S and 501 was very similar.

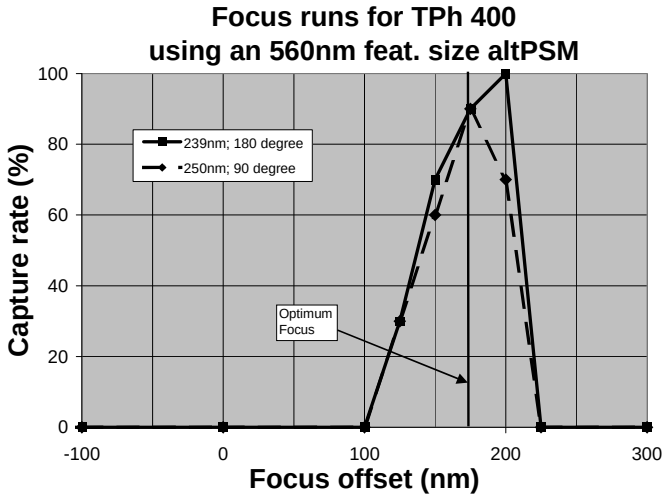

Fig. 2: Focus run for TPh 400 using an altPSM with feature sizes of 560 nm. For different defect types the capture rate for the smallest detected defect is plotted against the focus offset.

Fig. 2 shows the focus run for TPh 400 using an altPSM with feature sizes of 560 nm. The focus offset ranged from -300 nm to 300 nm at increments of 25 nm. Quartz defect heights of 60° and 30° were ignored in the analysis, as they were not detected consistently. Instead the capture rate of the smallest detected defect for defect heights of 180° and 90° is plotted against the focus offset. For on-edge bumps of 180° and 90° this maximum was achieved at focus offsets of 200 nm and 175 nm, respectively. The overall optimum focus offset, which was calculated from the average of the two values, was determined at 187 nm.

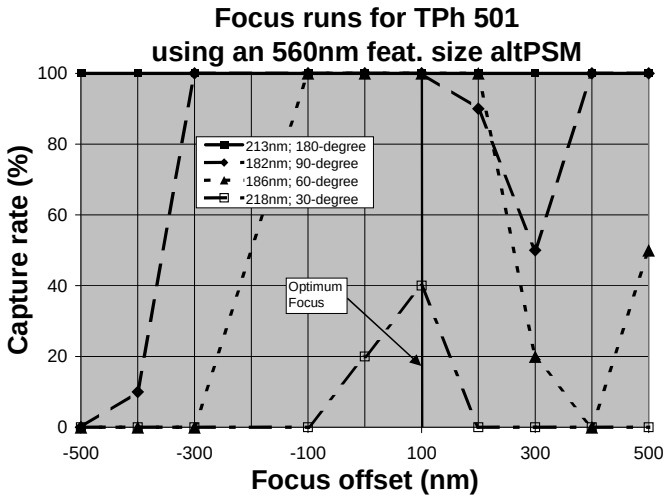

Fig. 3: Focus run for TPh 501 using an altPSM with feature sizes of 560 nm. For different defect types the capture rate for the smallest detected defect is plotted against the focus offset.

Fig. 3 shows the focus run for TPh 501 also using an altPSM with feature sizes of 560 nm. In general the smallest detected defect was much smaller than for TPh 400 (see also Fig. 5). For defect heights of 180°, 90°, and 60° the curves exhibit a plateau of 100 % capture rate. Due to the large increments in available defect sizes in this defect range the next smaller defect was not detected at all. A defined maximum is only observed for the defect height of 30° at 100 nm. The optimum focus offset was determined to be at 100 nm as all other curves at this point exhibit a 100 % capture rate.

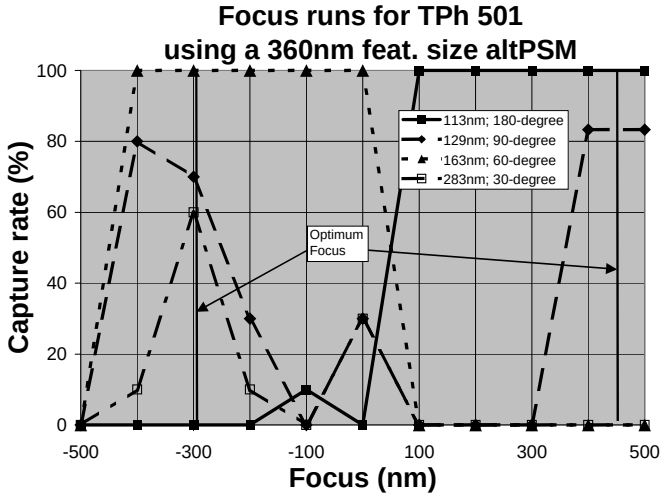

Fig. 4: Focus run for TPh 501 using an altPSM with feature sizes of 360 nm. For different defect types the capture rate for the smallest detected defect is plotted against the focus offset.

Additional focus runs were carried out for the altPSM with feature sizes of 360 nm. No analysis was done for TPh 400, as it didn't detect any of the programmed defects. Fig. 4 shows the results of the focus run performed for TPh 501 for focus offsets ranging from -500 nm to 500 nm at increments of 100 nm. For on-edge bumps of 180°, 90°, 60° and 30° the capture rate for the smallest detected defect was plotted against the focus offset. For defect heights of 180° and 60° the graph exhibits a plateau of 100% capture rate. Due to the lack of a smaller detected defect the optimum focus height for these defect types cannot be determined unambiguously. The optimum focus offset was determined through the maximums observed for defect heights of 90° and 30°, which are exhibited at -300 nm and approx. 450 nm. No single optimum focus could be determined in this case. In general the detectability of large quartz defect heights (180° and 90°) is higher at positive focus offsets, whereas shallow quartz defects (60° and 30°) are better detectable at negative focus offsets.

Optical simulations of quartz defects performed at different focus offsets show that quartz defects achieve a high image contrast both at negative as well a positive focus offsets. Depending on the focus offset the quartz defects appear either bright or dark against their surrounding. The dependence observed between the optimum focus offset and the quartz defect height could not be explained with the models applied and remains to be investigated.

It is interesting to note that for TPh 501 for feature sizes of 560 nm (see Fig. 3), 440 nm (data not shown), and 360 nm (see Fig. 4) the curve's absolute maximum for 30° on-edge bumps is exhibited at 100 nm, -300 nm, and -300nm, respectively. Clearly the optimum focus offset is also dependent on the feature size. At feature size of 560 nm a single optimum focus can be found (see Fig. 2). For feature sizes of 360 nm two focus settings are found necessary (see Fig. 4), which requires a two-path inspection.

3.2 DEFECT SENSITIVITY OF THE TERAPHASE ALGORITHMS

In a previous study it was found that TPh 400 exhibits feature size dependent defect sensitivity[6]. In this study we conducted comparable measurements with TPh 401S and TPh 501 using altPSMs with feature sizes of 560 nm, 440 nm, and 360 nm.

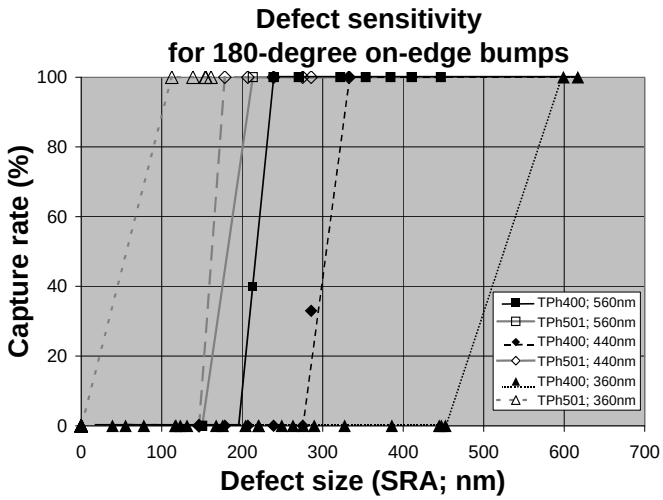

Fig. 5: Defect Sensitivity analysis of TPh 400 and TPh 501 for feature sizes of 560 nm, 440 nm, and 360 nm. The capture rates were plotted with respect to the defect size.

Fig. 5 shows a sensitivity comparison of TPh 400 and TPh 501 for 180° on-edge bumps. The measurements were performed at each algorithm's optimum focus offset. As previously observed the defect sensitivity of TPh 400 decreases with decreasing feature size. For feature sizes decreasing from 560 nm to 360 nm TPh 400's defect sensitivity decreases from 240 nm to above 320 nm. In comparison TPh 501 exhibits much higher defect sensitivity than TPh 400. Different than for TPh 400 the defect sensitivity actually increases with decreasing feature sizes. At feature sizes of 560 nm TPh 501 exhibits defect sensitivity below 213 nm and above 150 nm. At feature sizes of 440 nm the defect sensitivity fall in a similar range meaning below 180 nm and above 150 nm. At feature sizes of 360 nm the defect sensitivity is below 113 nm, which is well below the lower limit exhibited at features sizes of 560 nm and 440 nm.

It has to be stated that the observed increase in defect sensitivity of TPh 501 is only observed for 180° bumps. For 30° on-edge bumps and decreasing feature sizes from 560 nm to 440 nm the defect sensitivity of TPh 501 decreases from 240 nm to above 260 nm (see Tab. 1 and Tab. 2). A similar behavior is observed for 60° bumps.

As TPh 401S exhibits a similar behavior as TPh 501 it can be speculated that the defect detection method governs the observed defect sensitivity behavior. In general the optical contrast of the main features decreases with decreasing feature sizes. For the detection of quartz defects TPh 400 utilizes the reflected light, whereas TPh 401S and TPh 501 have a specialized phase-sensitive optics. For the reflected light the optical contrast of quartz defects behaves similar to a chrome defect and decreases with feature size. For the phase sensitive optics the phase shift contrast stays constant as the contrast of the surrounding main features decreases.

Sensitivity Table

0	102	150	213	239	270	322	353	384	bump edge	180
0	0	119	182	208	250	291	322	364		90
0	140	186	239	269	290	331	367	399		60
0	180	218	244	275	317	374	414	444		30

found 100% with TPh 400, 401S, and 501
found 100% with TPh 401S and 501
found 100% with TPh 501

Tab. 1: Sensitivity comparison of TPh 400, 401S, and 501 for feature sizes of 560 nm. In the vertical the defect height changes from 180°, 90°, 60° to 30°. The numbers in the squares give the defect size in nm. The square's color determines, which algorithm found the defect with a capture rate of 100 %.

Tab. 1 shows a defect sensitivity comparison of TPh 400, 401S, and 501. The increase in defect sensitivity for TPh 401S and 501 is most predominant for shallow quartz defects. At defect heights of 60° and 30° none of the programmed de-

fects was found by TPh 400. The phase sensitive optics of TPh 401S and 501 greatly enhances the detectability of these defects.

Sensitivity Table

0	0	146	178	207	239	275	286	333	bump on-edge	180
0	134	197	255	276	301	316	322	395		90
165	187	265	305	322	371	390	419	447		60
0	189	204	259	376	407	424	447	457		30

found 100% with TPh 401S and 501
found 100% with TPh 501

Tab. 2: Sensitivity comparison of TPh 401S and 501 for feature sizes of 440 nm. In the vertical the defect height changes from 180°, 90°, 60° to 30°. The numbers in the squares give the defect size in nm. The square's color determines, which algorithm found the defect with a capture rate of 100 %.

Comparing the performance of TPh 401S and 501 the advantage of the smaller inspection wavelength utilized for TPh 501 can be observed (see Tab. 1 and Tab. 2). It has to be noted that the defect size increments cause the sensitivity difference often not be measurable. In Tab. 1 for 180° and 90° the defect sensitivity of TPh 401S and 501 appears to be similar. For these defect types the actual sensitivity difference can be much better observed in Tab. 2, where the defect spacing close to the sensitivity roll-off is smaller. The opposite is observed for 30° defects, for which the defect sensitivity becomes visible in Tab. 2 but not in Tab. 1. Taking the data from Tab. 1 and Tab. 2 the improved defect sensitivity of TPh 501 becomes noticeable. TPh 501, which operates at an inspection wavelength of 257 nm, has a higher image resolution and therefore a higher defect sensitivity than TPh 401S, which operates a wavelength of 365 nm.

3.3 DEFECT PRINTABILITY STUDY FOR ALTPSMS

A defect printability study for altPSM was performed for feature sizes of 360 nm. Due to the complexity of the mask the printability study was limited to defect heights of 180°. Comparing the defect printability with the AIMS it was found that a 10 % CD wafer change corresponded to a 10 % AIMS intensity deviation.

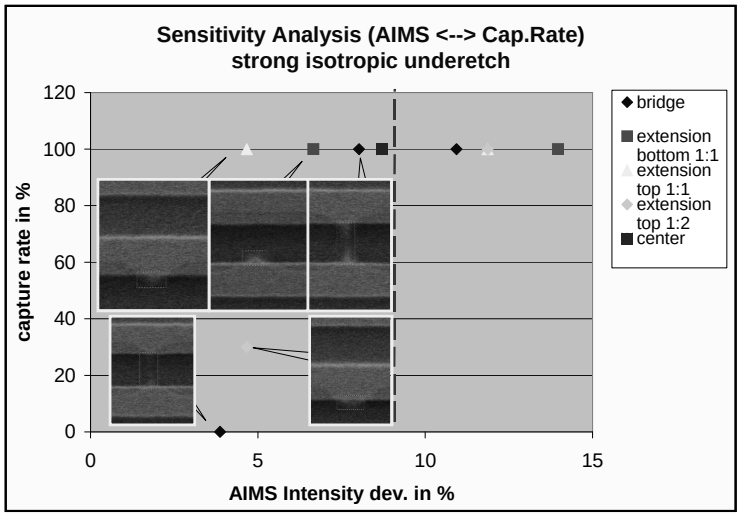

Fig. 6: Sensitivity analysis of TPh 401S for an intensity balanced altPSM, which was used in a defect printability study. The markers represent different types of programmed defects. The SEM images of critical quartz bumps are presented.

The same mask was also inspected with TPh 401S (see Fig. 6). The sensitivity analysis was performed at the optimum focus offset. For different defect types the capture rate, which represents the average of 10 inspections, was plotted against the AIMS deviation. The SEM images of defects with an AIMS intensity deviation below 10 % are shown. The

dotted vertical line marks the intensity deviation, above which all defects were found to be printing. For feature sizes of 360 nm TPh 401S and consequently also TPh 501 is capable of finding all printing 180° bumps.

Additionally a lithographic study for feature sizes of 440 nm was performed. The image, which was formed into the wafer resist, was scanned with a KLA wafer scan tool. So-called repeaters, which occurred in every single die were identified and traced back on the mask. It was found that there existed two large quartz defects, which had an approximate size of 2 µm (see Fig. 7). Scanning the defects with an AFM an approximate defect height of 20° was determined.

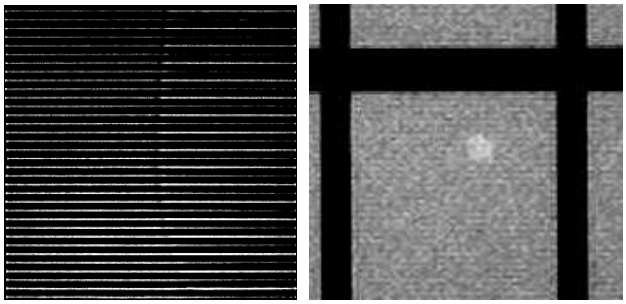

Fig. 7: Optical images of shallow quartz defects. The images were taken at approx. 1000x (left image) and 20x (right image) magnification.

Inspecting the mask with TPh 401S and 501 the defect could not be found. Driving the inspection stage to the defect locations and taking defect images at the inspection magnification the defect were not visible even when manually varying the optic's focus. As the defects exhibit a gradual edge transition the TeraPhase algorithms are not capable of locating the defect. Interestingly the defects became very visible, when looking at the defect with smaller optical magnification (see Fig. 7). It has to be noted that these image magnifications are only usable for defect review, but not for inspection of the mask surface.

3.4 INSPECTION OF CHROME-LESS PSMS

One of the major challenges for the inspection of chrome-less PSMs is the inspection tool's light calibration. Before any inspection the imaging optics' gain and offset needs to be adjusted such that the inspection images taken during the scanning of the mask don't become saturated. For a proper light calibration the tool needs two large areas, each of which consist of bright and dark areas. For a chrome-less PSM only dark lines can be generated. Large dark areas have to be realized through a very close spacing of etched and un-etched quartz areas.

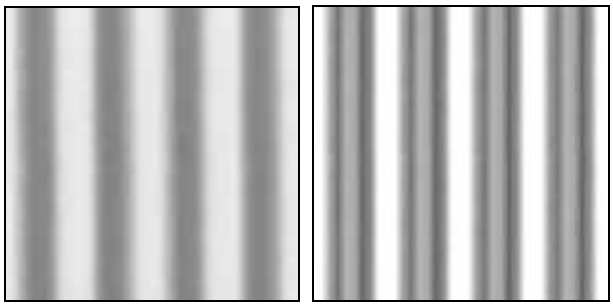

Fig. 8: Images of a chrome-less PSM taken with TPh 401S (left) and TPh 501 (right).

As no such dark areas were available, the light calibration was performed for large chrome and quartz patches. Fig. 8 shows images of the chrome-less PSM taken with TPh 401S and TPh 501. In the image taken with TPh 401S the bright and gray lines represent the un-etched and etched quartz, respectively. The dark lines, which are generated in the aerial image of the lithography wavelength through destructive interference at the transition from the etched to the un-etched quartz, don't become visible. For the image taken with TPh 501 the bright and gray lines also correspond to the un-etched and etched quartz, respectively. Additionally between the bright and gray lines the image contains dark lines, which exhibit resemblance to the dark lines in the aerial image at the lithography wavelength of 193 nm.

The chrome-less PSM was inspected both with TPh 401S and 501 (see Fig. 9). The inspections were performed at maximum sensitivity settings and the optimum focus offset, which had been determined with the altPSM test masks.

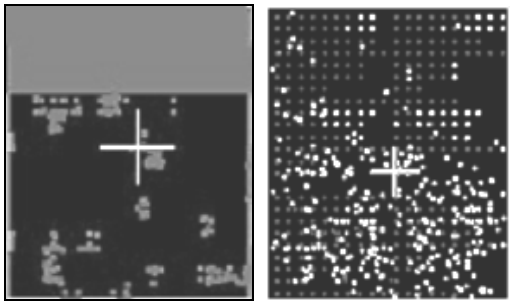

Fig. 9: Defect maps of the defects found with TPh 401S (left) and 501 (right), when inspecting a chrome-less PSM with programmed defects.

Defect inspection with TPh 401S triggered massive false defects. Due the performed light calibration the image contrast was considerably low. This caused the tool to often loose it's dynamic alignment during inspection triggering massive false defects a the boundaries of a chrome-less phase shift field. An evaluation of the programmed defect section was not possible.

The inspection of TPh 501 was completed without any false defects. The algorithm found numerous programmed and process defects. The programmed defects, which were located in the top half of the inspection field, can be easily identified by the regular spacing between the defects. It can be concluded that TPh 401S is not suitable for the inspection of such chrome-less PSMs. TPh 501 instead showed promising inspection results for such masks. A sensitivity analysis was not performed, as the programmed defect had not been characterized. A sensitivity analysis of TPh 501 for chrome-less PSMs will be the subject of future investigations.

4 SUMMARY

The algorithms TPh 401S and 501 exhibit a significant quartz defect sensitivity improvement in comparison to TPh 400. Whereas for TPh 400 the defect sensitivity decreases for decreasing feature sizes the defect sensitivity of TPh 401S and 501 in the range from 560 nm to 360 nm was found to be independent of the feature size. The sensitivity difference between TPh 400 and TPh 401S/501 is therefore greatest for the smallest utilized feature size of 360 nm. For 180° bumps the defect sensitivity of TPh 400 is above 320 nm, whereas TPh 501 exhibited a defect sensitivity of approx. 113 nm.

Comparing the performance of TPh 501 and 401S, TPh 501 has a clear wavelength advantage. The utilized inspection wavelength of 257 nm vs. 365 nm allows for a better image resolution and consequently achieves higher defect sensitivity. At defect heights of 180°, 90°, 60°, and 30° the sensitivity improvement is the range of 30 to 50 nm.

Focus runs performed for all three algorithms showed that the optimum focus offset depends on the quartz defect height as well as the feature size. For large feature sizes, the focus run maximums appear at similar focus offsets. For smaller feature sizes defect heights of 180° and 90° are better detectable at positive focus offsets, whereas defect heights of 60° and 30° are better detectable at negative focus offsets. Consequently a two-path inspection is needed to achieve maximum sensitivity for all defect heights studied.

TPh 401S and 501 were capable of detecting all 180° bumps, which had been considered printing, in a defect printability study for feature sizes of 360 nm. An exception was found for very shallow quartz defects. These fairly large defects with a gradual edge transition had been found printing, but could not be detected with neither TPh 401S nor 501.

TPh 501 proved very suitable for the inspection of chrome-less PSMs. Captured images show a resemblance to the aerial image at the lithography wavelength. The algorithm exhibited good inspectability of a programmed defect test mask.

ACKNOWLEDGEMENTS

This work was supported by the German Federal Ministry of Education and Research (BMBF) under Contract No. 01M3154A.

REFERENCES

1. M.D. Levenson, N.S. Viswanathan, and R.A. Simpson; “Improving Resolution with a Phase-Shifting Mask”, IEEE Trans. Elect. Dev., ED 29, pp. 1828-1836 (1982)
2. K.K.H. Toh et al., “Chrome-less phase-shifted masks: A New Approach to Phase-Shifting Masks”, *Proceedings of SPIE*, Vol. 1496, pp. 27-53, SPIE, 1990
3. K.K.H. Toh et al., “Optical Lithography with Chrome-Less Phase-Shifted Masks”, *Proceedings of SPIE*, Vol. 1463, pp. 74-86, SPIE, 1991
4. J. Thiele, M. Ahrens, W. Dettmann, M. Heissmeier, M. Hennig, B. Ludwig, M. Moukara, R. Pforr; “Introduction of Full Level Alternating Phase Shift Mask Technology into IC Manufacturing”; *Proceedings of SPIE*, Vol. 4691, SPIE, 2002
5. L. Zurbrick, J. Heumann, M. Rudzinski, S. Stokowski, J.P. Urbach, and L. Wang, “New Approaches to Alternating Phase Shift Mask Inspection”, *Proceedings of SPIE*, Vol. 4562, pp. 138-144, SPIE, 2002
6. J. Heumann, M. Zarrabian, M. Hennig, W. Dettmann, L. Zurbrick, and M. Lang;” AltPSM Inspection Capability and Printability of Quartz Defects”, *Proceedings of SPIE*, Vol. 4889, pp. 1033-1040, SPIE, 2002
7. L. Zurbrick, M. Rudzinski, L. He, K. Kimmel, A. Williams, “Phase Enhanced DUV Inspections of Alternating Phase Shift Reticles”, *Proceedings of SPIE*, Vol. 5256, pp. 1174-1180, SPIE, 2003
8. L. Zurbrick, J. Heumann, M. Rudzinski, S. Stokowski, J.P. Urbach, and L. Wang, “New Approaches to Alternating Phase Shift Mask Inspection”, *Proceedings of SPIE*, Vol. 4562, pp. 138-144, SPIE, 2002
9. L. Zurbrick, J. Heumann, M. Rudzinksi, S. Stokowski, J.P. Urbach, and L. Wang, “Alternating Phase Shift Mask Inspection Using Multiple Simultaneous Illumination Techniques”, *Proceedings of SPIE*, Vol. 4754, pp. 511-516, SPIE, 2002